



Article

Synthesis and Characterization Bimetallic Organic Framework CoxFex(BDC) and Adsorption Cationic and Anionic Dyes

Thi Kim Ngan Tran ^{1,2,*} , Cao Phuong Khanh Phan ³, Thi Cam Quyen Ngo ^{1,2}, Ngoc Bich Hoang ^{1,2} ,
Le Dang Truong ^{1,2} and Thi Kim Oanh Nguyen ^{1,2}

¹ Institute of Applied Technology and Sustainable Development, Nguyen Tat Thanh University, Ho Chi Minh City 700000, Vietnam; ntcquyen@ntt.edu.vn (T.C.Q.N.); bichhn@ntt.edu.vn (N.B.H.); ldtruong@ntt.edu.vn (L.D.T.); ntcoanh@ntt.edu.vn (T.K.O.N.)

² Faculty of Food and Environmental Engineering, Nguyen Tat Thanh University, Ho Chi Minh City 700000, Vietnam

³ Faculty of Chemical Engineering, Ho Chi Minh City University of Technology, Ho Chi Minh City 70000, Vietnam; khanh.phan_stayfresh@hcmut.edu.vn

* Correspondence: ngantk@ntt.edu.vn; Tel.: +84-765-712-086

Abstract: Co-doped Fe-MOF bimetallic organic framework materials at different ratios were synthesized based on the solvothermal method, and we evaluated their morphological characteristics by modern analytical methods such as SEM, XRD, FT-IR, and isotherm of nitrogen adsorption-desorption (BET). The specific surface area of the 0.3 CoFe-MOF sample (280.9 m²/g) is much larger than the Fe-MOF and samples at other ratios. The post-synthesized materials were evaluated for their ability to absorb various dyes, including Methylene Blue (MB), Methyl orange (MO), Congo red (CR), and Rhodamine (RhB), and evaluated for the effects of pH, the initial concentration of the dye solution, time, and dose of adsorbent. The results show that the 0.3 CoFe-MOF material has a high adsorption capacity that is superior to both the original Fe-MOF and the CoFe-MOFs at other ratios. The highest adsorption capacity of MB dye by 0.3 CoFe-MOF reaches up to 562.1 mg/g at pH 10, the initial concentration of MB of 200 mg/L, after 90 min. The charged properties of the dyes and the charged nature of the bimetallic organic frameworks are best demonstrated through the adsorption of dye mixtures. The adsorption efficiency on the mixed system of cationic (MB) and anionic (MO) dyes yielded the highest removal efficiency of 70% and 81%, respectively, after 30 min. Therefore, the research has opened up the potential application of M/Fe-MOF modified materials and CoFe-MOF in organic dyes adsorption in wastewater treatment for environmental protection.

Keywords: bimetallic organic framework; adsorption; dye mixture; cation dye; anion dye



Citation: Tran, T.K.N.; Phan, C.P.K.; Ngo, T.C.Q.; Hoang, N.B.; Truong, L.D.; Nguyen, T.K.O. Synthesis and Characterization Bimetallic Organic Framework CoxFex(BDC) and Adsorption Cationic and Anionic Dyes. *Processes* **2022**, *10*, 1352. <https://doi.org/10.3390/pr10071352>

Academic Editor: Avelino Núñez-Delgado

Received: 11 June 2022

Accepted: 5 July 2022

Published: 12 July 2022

Publisher's Note: MDPI stays neutral with regard to jurisdictional claims in published maps and institutional affiliations.



Copyright: © 2022 by the authors. Licensee MDPI, Basel, Switzerland. This article is an open access article distributed under the terms and conditions of the Creative Commons Attribution (CC BY) license (<https://creativecommons.org/licenses/by/4.0/>).

1. Introduction

With the continuous development of science and technology, the studies of new types of material that exhibit more outstanding features than zeolite, activated carbon, or other microcapillary materials, termed the framework material metal-organic, have been extended. This is a material with a porous structure and a very large specific surface area (2000–6500 m²/g) built on a metal-organic framework (MOFs) [1]. The MOFs materials contain both medium and micro-capillary and are usually synthesized by the hydrothermal method. In addition, they are also synthesized by other methods such as microwave, ultrasonic, chemical treatment, and electrochemistry. The combination of organic and inorganic substances can form different types of MOFs with many unique properties.

MOFs are porous solid crystalline materials with spatially extended one-dimensional to three-dimensional structures formed from the “assembly” of metal ions or clusters. Oxides associated with ligands are organic bridges [2–4]. This material has attracted considerable attention due to its large specific surface area, thermal stability, structural diversity as well as highly ordered structure, leading to many applications in various fields such as storage gases, catalysts, sensors, drug delivery, and biomedicine [5–9]. Specifically,

the synthesis of the physical and chemical properties of MOFs can be tuned by incorporating functional groups on organic bonds or metal unsaturated sites in the lattice of MOFs.

In particular, the modification of MOF materials remains of interest to research on the synthesis process and its applications. Currently, there are two commonly used methods to modify materials, including (i) introducing transition metal or metal oxide into the material, and (ii) attaching the organic functional groups onto the capillary surface [10–12]. Therefore, the potential applications of MOF materials attached with some oxides to their frame have not been exploited much. The applications of this MOF material are adsorption of heavy metal and dye in solution, catalysis for oxidation reactions of organic compounds, and photocatalysts, which exhibit practical significance.

For example, Hossein et al. (2018) removed both anionic (MO) and cationic (MB) dyes by MOF based on Zirconium (UiO-66) [13]. Mantasha et al. (2020) evaluated the dye adsorption process to separate MB from a mixture of three dyes in an aqueous solution (i.e., MO, RhB, and MB) by Cu-centered MOF (Cu-MOF). By comparing the adsorption capacity of anionic and cationic dyes, results also showed that the surface of anionic-charged materials would better adsorb cationic dyes and vice versa [14]. Similarly, the cationic MOF material (SCNU-Z1-Cl) was successfully synthesized by the combination of organic ligand containing N_2 and metal ion Ni^{2+} with a high specific surface area ($1636\text{ m}^2/\text{g}$) and was able to remove the anionic dyes (CR, MO, and OA) and anionic oxo pollutants ($Cr_2O_7^{2-}$, CrO_4^{2-} , and MnO_4^{2-}) in just minutes to 1 h [15]. Moreover, MO is an acidic anionic dye that exists in various wastewater sources such as pharmaceuticals, textiles, and printing, directly affecting the environment and aquatic organisms. Carcinogenic benzidine compounds are formed by some aromatic amines in the MO dye structure after bioconversion [16]. Another anionic dye known as Congo red (CR), which is widely used in the plastic and rubber industry, is directly harmful to the environment, yet it is difficult to degrade due to naphthalenes and benzene rings in the structure [17]. On the other hand, MB is a cationic dye that directly affects human health and the natural aquatic environment if it is not properly treated [18]. The potential applications of MB range from pharmaceutical, dyeing, drug, and printing to coating and food industries. MB is most commonly used in the textile industry due to its strong and durable properties in the fiber's structure. However, MB at a high concentration can cause skin irritation, nausea, respiratory depression, and digestive disorders upon direct exposure [19]. Similarly, with the nature of a cationic dye and complex structure, the presence of RhB in wastewater from the dyeing, textile, and paint industries is considered a tremendous challenge for treatment. RhB has been found as a source of skin diseases, cancer, and alteration to kidneys and liver function when an excess of dye is released into the aquatic environment [20].

Therefore, the present study attempted to synthesize Co/Fe-MOF bimetallic modified materials based on the solvothermal method by combining metal salts and ligand Benzene-1,4-dicarboxylic acid. The structural, morphological, and physicochemical properties of the synthesized materials were obtained by modern physicochemical methods such as X-ray diffraction analysis (XRD), Fourier-transform infrared spectroscopy (FT-IR), scanning electron microscopy (SEM), and Brunauer–Emmett–Teller surface analysis (BET). These findings provided insights to improve the potential application of the material as an adsorbent in the process of removing toxic organic pigments (Figure 1) in the aquatic environment.

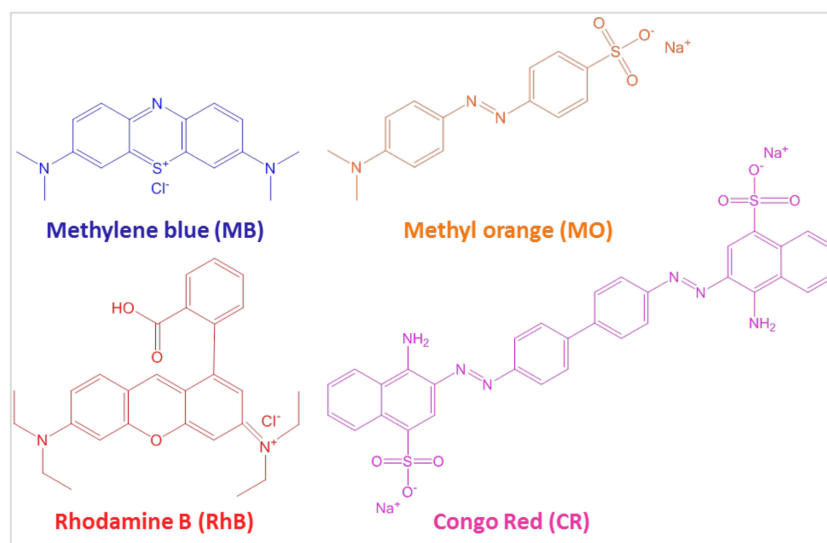


Figure 1. Chemical structures of cationic and anionic dyes in the study.

2. Materials and Methods

2.1. Materials

A Terephthalic acid (H_2BDC , Sigma-Aldrich Co. (St. Louis, MO, USA), N,N-dimethylformamide (DMF), ethanol ($\text{C}_2\text{H}_5\text{OH}$), iron (III) chloride hexahydrate ($\text{FeCl}_3 \cdot 6\text{H}_2\text{O}$), cobalt nitrate hexahydrate ($\text{Co}(\text{NO}_3)_2 \cdot 6\text{H}_2\text{O}$) were obtained from Xilong Chemical Co., Ltd. (Shantou, China)). Methyl Blue (MB), Methyl Orange (MO), Congo Red (CR), and Rhodamine B (RhB) were purchased from Sigma-Aldrich Co. (St. Louis, MO, USA).

2.2. Synthesis of Fe-MOF Doped Co

The synthesis of Fe-MOF was carried out using solvothermal method according to previous research by Ding et al. (2021) [21], with slight modifications. A total of 5 mmol H_2BDC and 10 mmol $\text{FeCl}_3 \cdot 6\text{H}_2\text{O}$ was added to a 60 mL DMF beaker and stirred magnetically for 30 min. The solution was then placed into Teflon for heating at 150°C for 20 h and cooled down to room temperature. Next, the mixture was centrifuged at $6000 \times g$ for 10 min. The solid was collected and the remaining solution was washed with DMF and Ethanol solvents. Finally, the material sample was dried using vacuum at 120°C overnight. Subsequently, the materials were post-modified with Co^{2+} ions at different molar ratios (10%, 30%, and 50%) in order to investigate the influence of the amount of Co metal introduced on the adsorption capacity of Co^{2+} ions.

2.3. Characterization of the Materials

Structure and surface morphology of material samples were investigated through SEM images (Hitachi S-4800, Tokyo, Japan). X-ray diffraction (XRD) was used to study the crystalline phase composition of the materials when synthesized and denatured under different conditions, using (D8 Advanced— Bruker, Billerica, MA, USA) at $\text{Cu K}\alpha$ radiation ($\lambda = 1.54188 \text{ \AA}$). The functional groups of organic compounds were based on the FT-IR method using Nicolet 6700 (FTIR Affinity-1S, Shimadzu, Tokyo, Japan). Several parameters of porous materials such as specific surface area, size, and pore volume were measured using the N_2 adsorption-desorption isotherm (BET) method via Micromeritics 2020—Micromeritics, Norcross, GA, USA. The concentration of the toxic organic pigment solution during the adsorption capacity of the material was analyzed using a UV-Vis spectrophotometer (Thermo, Evolution 60S, Waltham, MA, USA).

2.4. Dye Adsorption Experiments

The dye adsorption process was investigated in batch experiments with various time periods to reach the adsorption equilibrium (10–300 min). The influence of the solution pH was tested in the range of 2–12, pH was adjusted based on 0.1 M HCl and NaOH solution. An exact dose of adsorbent (0.002–0.03 g/L) was weighed into Erlenmeyer containing 50 mL of dye solution with a concentration of 30–300 mg/L. After certain time intervals, 4 mL of sample was centrifugated at $6000 \times g$ for 5 min. After the solids were removed, the remaining solution was determined by UV-Vis. The adsorption capacity (mg/g) of dye after adsorption was calculated by the following formula:

$$q_e = \frac{(C_0 - C_e)V}{m}$$

where q_e (mg/g) is the adsorption capacity of the dye at the time of equilibration, C_0 (mg/L) is the initial dye concentration, C_e (mg/L) is the dye concentration at equilibration time, m (g) is the dose of adsorbent and V (L) is the volume of dye solution.

2.5. Reusability of the Adsorbent

The most suitable adsorbent material and dyes were selected for the experiment to investigate the reusability. The selected adsorbent was recovered, then filtered and washed with ethanol and dried at 120 °C for 12 h.

3. Results and Discussion

3.1. Characterization of Materials

The crystalline phase growth and composition of Fe-MOFs samples were modified with Co at different Co: Fe molar ratios: 0.1, 0.3, and 0.5 and were analyzed by XRD. The results of Figure 2A showed that the Fe-MOF sample exhibited the characteristic diffraction peaks at 2θ of 12.5°, 16.2°, 18.9°, and 22.08°, respectively, which corresponded to the study of Xie et al. (2017) [22]. All three Fe-MOF samples modified with Co showed similar characteristic peaks, indicating that the bimetallic materials have been successfully synthesized on the Fe-MOF background. They have an almost similar crystal structure, despite some slightly different peak intensities. The difference in the position of the characteristic diffraction peaks is due to the introduction of the second metals into the synthesized Fe-MOF bimetallic structure, but the peaks retain their sharpness, specifically when compared between CoFe-MOF doped samples and Fe-MOF samples. The high intensity at the 12.5° diffraction peak shifts to a lower angle, while the 16.2° peak shifts to a higher angle as the Co/Fe ratio increases, because the radius of Co^{2+} (65 nm) is larger than the radius of Fe^{3+} (64 nm). The presence of the second metal in the bimetallic structure has led to the difference in characteristic diffraction peaks, which has also been reported in a few publications previously [7,23]. Co-doping with a larger ionic radius than Fe^{3+} increases the lattice constant, causing the theta angle to shift lower. At the same time, the appearance of displacements in both directions (lower and higher angles) is often due to flexibility or the breathing effect of the structure [24].

Figure 2B shows that as a result of FT-IR analysis of Fe-MOF and CoFe-MOF, the characteristic peaks of Fe-MOF appear at 527, 751, 1393, 1589, and 3607 cm^{-1} , respectively. The peaks ranged from 3000 to 3700 cm^{-1} from –OH in water molecules adsorbed on the surface of the material. The FT-IR spectrum shows a strong peak at 1393.1589 cm^{-1} corresponding to the symmetrical and asymmetrical oscillations of the carboxylic group in the BDC coordinated with cobalt and iron ions. The absorption peaks at 527 and 751 cm^{-1} come from the bond formed by Fe^{3+} , the carboxylic acid functional group (Fe-O), and characterize the C-H bond vibration of the benzene ring [25]. Basically, the characteristic peaks of CoFe-MOF are similar to those of Fe-MOF, with only some displacement and size of the peak of 662 cm^{-1} , which may be caused by the carboxyl group in terephthalic acid and Co^{2+} [26].

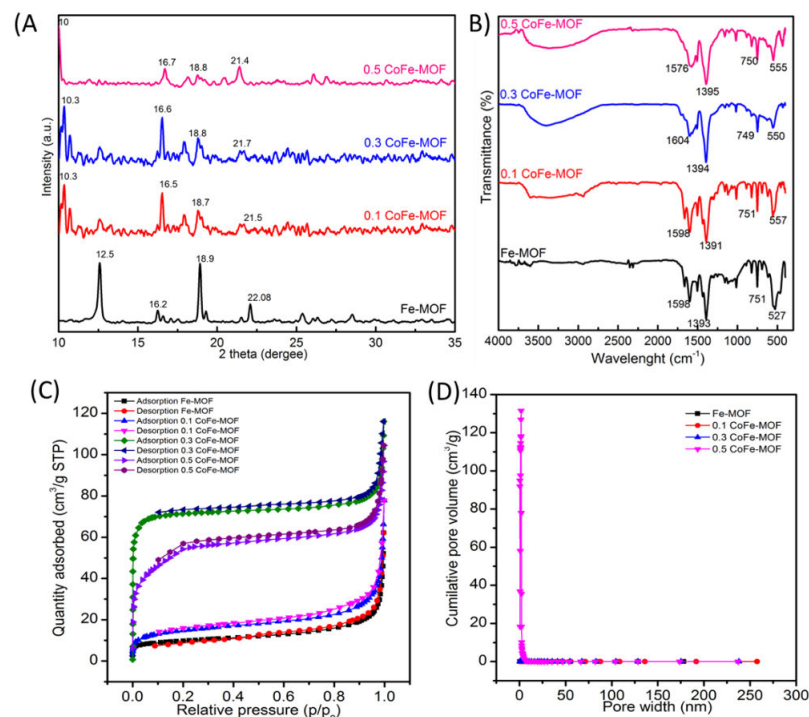


Figure 2. (A) XRD pattern, (B) Fourier transform infrared spectra (FT-IR), (C,D) Nitrogen adsorption/desorption isotherms of Fe-MOF and CoFe-MOF at different ratios.

The results of Figure 2C,D show that the desorption curve has typical type II isotherm characteristics (according to IUPAC classification) that characterize the presence of a small capillary type. The S_{BET} of Fe-MOF, 0.1 CoFe-MOF, 0.3 CoFe-MOF, and 0.5 CoFe-MOF were of 32.8, 52.6, 280.9, and 189.5 m^2/g , respectively. Table 1 shows that the BET surface area of Fe-MOF of 32.8 m^2/g increases to 280.9 m^2/g when changing the center of the second metal in the lattice with a molar ratio of 0.3 Co:Fe. At the same time, the pore diameter and pore volume also change, creating suitable conditions for rapid diffusion of the adsorbed substances to the adsorption centers of the adsorbent, thereby increasing the adsorption capacity [25]. The specific surface area of the material is also affected by the change in the material morphology in the presence of Co^{2+} ions; the crystal morphology changes from axial rotation to octahedral with two pointed ends, resulting in a larger specific surface area [27].

Table 1. BET data of Fe-MOF and CoFe-MOF.

| Sample | BET Surface Area (m^2/g) | Porous Diameter (nm) | Porous Volume (cm^3/g) |
|--------------|--|----------------------|--|
| Fe-MOF | 32.8 | 7.9 | 0.06 |
| 0.1 CoFe-MOF | 52.6 | 6.5 | 0.09 |
| 0.3 CoFe-MOF | 280.9 | 2.2 | 0.15 |
| 0.5 CoFe-MOF | 189.5 | 2.8 | 0.14 |

The morphology of all Fe-MOF and CoFe-MOF materials exhibit typical octahedral shapes with an average diameter of about 2 μm (Figure 3) [28]. When changing the molar ratio of Co:Fe, uneven structure distribution, crystal size change, or deformation was observed. At the doping ratio of 0.3 Co:Fe, the crystals formed are well-defined and homogeneous octahedrons with apical tips at the two pointed ends. Furthermore, increasing the 0.5 Co:Fe doping ratio has resulted in crystals with a long rod-like shape. The rough and angular crystal surface is more obvious when some Fe metal centers are replaced by the presence of Co metal in the structure and the Co^{2+} radius is larger than Fe^{3+} , leading to a large surface area of CoFe-MOF as compared to the Fe-MOF single metal material.

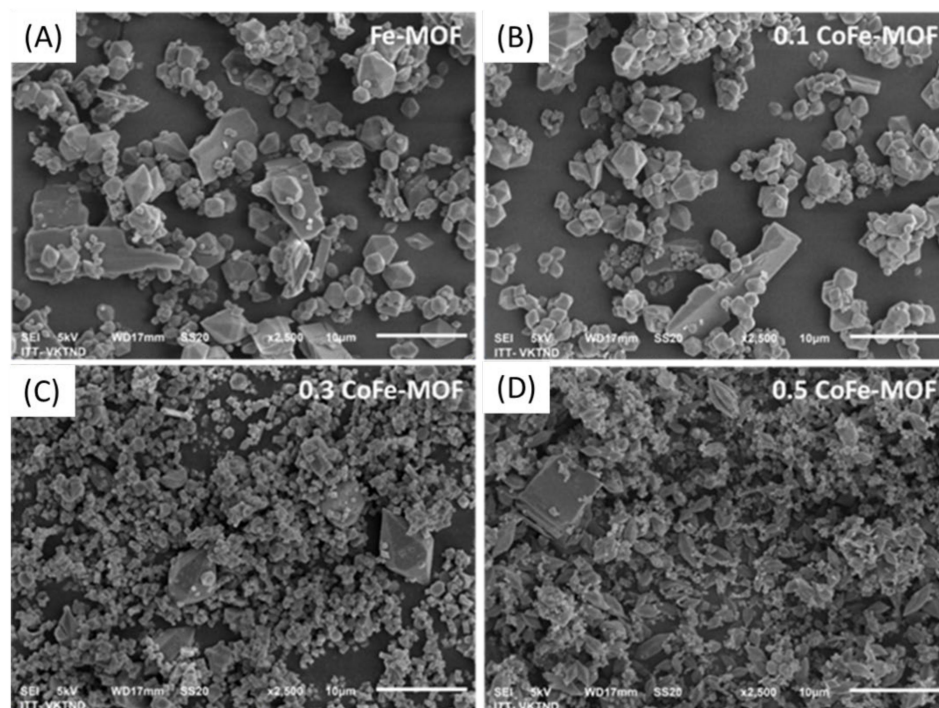


Figure 3. SEM images of (A) Fe-MOF, (B) 0.1 CoFe-MOF, (C) 0.3 CoFe-MOF and (D) 0.5 CoFe-MOF.

3.2. Effect of Co/Fe Ratios and pH Value on Zeta Potential on Dye Removal

The adsorption capacity of the synthesized materials, including Fe-MOF; 0.1 CoFe-MOF; 0.3 CoFe-MOF; 0.5 CoFe-MOF in dye adsorption were compared at the initial concentration of 30 mg/L; the amount of adsorbent 0.01 g/L; adsorption time is 90 min; pH 10 (MB and RhB) and pH 4 (MO and CR). As shown in Figure 4A, compared to the Fe-MOF materials, the CoFe-MOF at all $n\text{Co}^{2+}/n\text{Fe}^{3+}$ ratios yields high adsorption capacity compared to the starting material and adsorption equilibrium after 90 min. The 0.3 CoFe-MOF sample produces the highest adsorption efficiency, with an adsorption capacity of about 319.2 mg/g MB, 41.3 mg/g RhB, 116.2 mg/g MO, and 162.5 mg/g CR. The increasing adsorption capacity of the material after modification is due to the increase in the specific surface area and pore size of the material, so the material was able to absorb a large number of organic pigments on the surface and inside the pore. Moreover, the carboxyl group reacts simultaneously with two metal ions, and the large Co^{2+} radius of approximately 65 nm increases the surface area and contact area of the sample, thereby increasing the adsorption capacity [27].

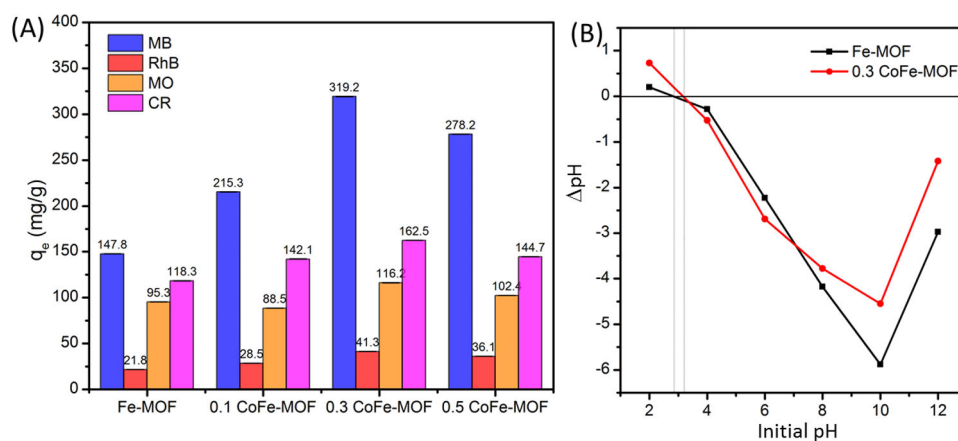


Figure 4. (A) Dye adsorption capacity at different rates, (B) Point of zero charge (pH_{pzc}) of Fe-MOF and CoFe-MOF.

The formation of surface charge on the adsorbent and the ionization of the adsorbent in solution are the two factors that are governed by the pH value as they control the electrostatic interaction between the adsorbents [29]. In general, the MB pigments were adsorbed better in the basic pH medium than at low pH in both materials, which could be explained by the pH point of zero charges (PZC).

Specifically, based on the study of Tran et al. (2020), 5 mg of adsorbent was weighed and added to Erlen containing 50mL of 0.1M KCl solution at different initial pH values (2, 4, 6, 8, 10, 12). The solutions were shaken for 24 h at 200 rpm at room temperature, then centrifuged at $6000 \times g$ for 10 min to remove the solids from the mixture. The pH_{pzc} of the material is the intersection point between the initial pH and the latter, which is determined at the value $\Delta pH = 0$. The survey results are shown in Figure 4B, in which the pH_{pzc} values of the Fe-MOF and 0.3 Co/Fe-MOF materials are 2.9 and 3.2, respectively. If the pH is greater than pH_{PZC}, the surface of the adsorbent becomes negatively charged, as it reacts at high pH to produce H^+ protons. For pH values below pH_{PZC}, the adsorbent surface carries a positive charge because the reaction at low pH produces OH^- hydroxide group [30].

3.3. Effect of Operating Parameters on Dye Adsorption Capacity

The influence of pH on the adsorption capacity of 0.3 CoFe-MOF dyes is also mentioned here. In general, the surface charge formation on the adsorbent and adsorption ionization in solution are the two factors that are dominated by the pH value as they control the electrostatic interaction between the adsorbents. In this study, different pH values from 2–12 while the concentrations of initial dye and adsorbent were maintained at 30 mg/L and 0.01 g/L, respectively. The contact time for the cationic and anionic dyes were 90 min and 60 min, respectively. Note that the acidity, alkalinity, or neutrality of MB solution can be easily adjusted using NaOH and HCl solutions. As shown in Figure 5A, the best absorption of 0.3 CoFe-MOF occurred in high pH environments and peaked at 396.4 mg/g at the optimum pH of 10. At very low pH values (i.e., pH 2), the adsorption efficiency was 164.85 mg/g.

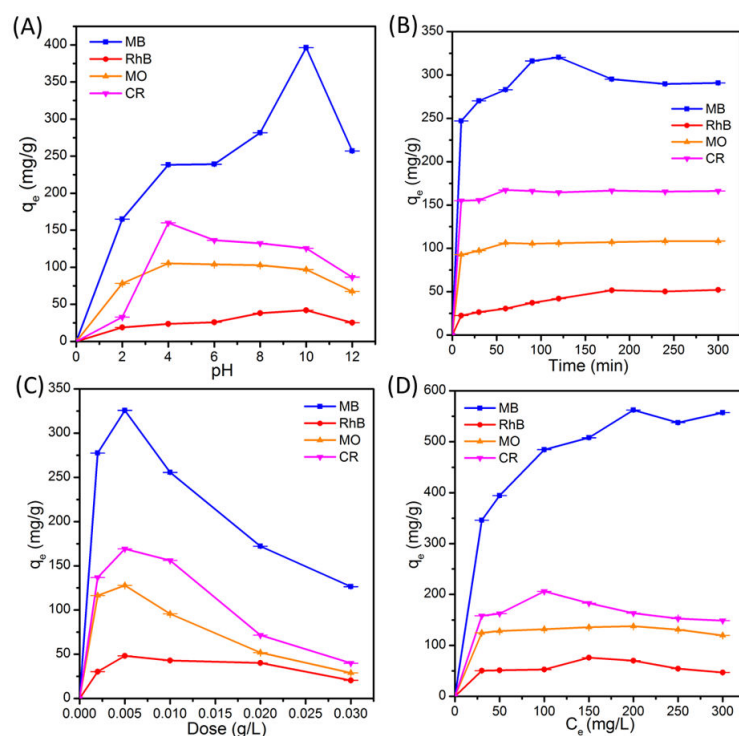


Figure 5. Effects of (A) pH, (B) contact time, (C) adsorbent dose, and (D) dye initial concentration on the dye adsorption capacity by 0.3 CoFe-MOF.

As depicted in Figure 5B, the adsorption process took place within the period from 10 to 300 min, while other experimental conditions were kept constant. The results showed that when increasing the adsorption time, the adsorption capacity of 0.3 Co/Fe-MOF also increased rapidly and gradually approached the equilibrium state at 316.15 mg/g (MB) from 90 min onwards. In contrast, all RhB, MO, and CR dyes reached equilibrium from 60 min, but the adsorption capacities were relatively low at only 30.6 mg/g, 106.21 mg/g, and 159.85 mg/g, respectively. In the beginning, the MB pigment adsorption and diffusion processes of the material occur rapidly due to the large external contact area. When the surface area of the material reaches saturation point, the pigment molecules enter the gaps of the adsorbent and are adsorbed by the inner surface. When further increasing the contact time, the adsorption capacity increased slightly, and then the desorption process also took place immediately because the dye content on the material was greater than the dye content in the solution.

Figure 5C illustrated the effect of the adsorbent dosage on the adsorption capacity of 0.3 CoFe-MOF to remove cationic and anionic dyes. When increasing the adsorbent dosage from 0.002 g/L to 0.03 g/L under the remaining constant conditions, the ability to remove dyes was obtained in the order of MB > CR > MO > RhB. Specifically, the results showed that the highest adsorption capacity in MB was 277.5 mg/g after 90 min of reaction at the dose of 0.002 g/L. When increasing the amount of adsorbent to 0.005 g/L, the MB adsorption capacity increased significantly to 325.8 mg/g after 90 min of reaction. However, the adsorption capacity tends to decrease when the amount of 0.3 CoFe-MOF increases from 0.01 to 0.03 g/L, the adsorption capacity tends to decrease for both types of adsorbents. This can be explained due to the fact that in the presence of a small amount of adsorbent, the number of reactant molecules is higher than the number of reaction centers, so when increasing the amount of adsorbent, the reaction rate and the adsorption efficiency increase. However, an excessive amount of adsorbent would reduce the adsorption center due to the collision and contact between the particles. It can be seen that the increasing removal of dyes in solution in response to increasing adsorbent mass is due to the increasing surface area and the number of adsorption sites in the materials. However, if too much adsorbent is used, agglomeration can occur, thereby reducing the total surface area of the material and leading to poor adsorption capacity.

In order to evaluate the best adsorption capacity of 0.3 CoFe-MOF for the dyes, the effects of the initial solution concentration of MB, MO, RhB, and CR dyes (30–300 mg/L) on the adsorption capacity were investigated. Figure 5D shows that the dyes were adsorbed very quickly at the range of 30–50 mg/L of initial concentration, then continued to be strongly adsorbed as the concentration increased to 200 mg/L, and finally decreased at the initial concentrations of 250 mg/L and 300 mg/L. On the other hand, when increasing the initial concentration of MO, RhB, and CR dyes (100–300 mg/L), the adsorption capacity tends to decrease and no significant difference was observed. It is possible that as the dye concentration increases, the mass transfer kinetics increase. Also, while low initial concentrations provide vacant active sites on the adsorbent surface, exceeding this point would require more active sites for the adsorption of color molecules, thus slowing down the adsorption process and decreasing the adsorption capacity.

3.4. Reusability of 0.3 CoFe-MOF

Based on the results obtained from the survey on the influence of the adsorption process of the dyes, MB was selected to evaluate the reusability of 0.3 CoFe-MOF material studied through the number of MB adsorption cycle times. Figure 6 shows that the adsorption capacity of 0.3 CoFe-MOF remained relatively unchanged at over 400 mg/g over four times of recycling. The slight decline in the adsorption capacity of 0.3 CoFe-MOF after multiple cycles is possibly due to the masking of the adsorption center by MB dye.

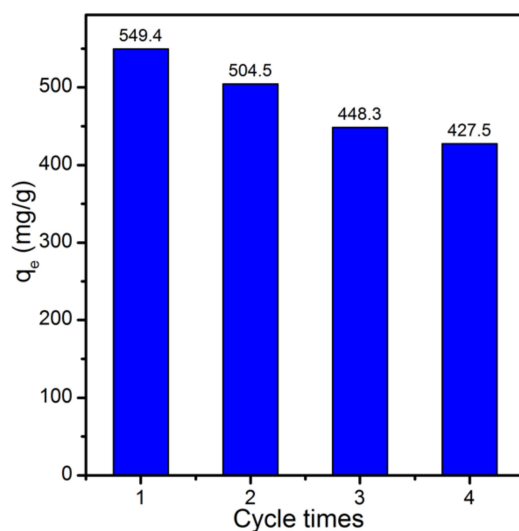


Figure 6. Q_e (mg/g) of 0.3 CoFe-MOF after four recycles.

3.5. Adsorption Kinetics

The rate of dye adsorption (MB, RhB, MO, and CR) above 0.3 CoFe-MOF was studied during the adsorption equilibrium time. The obtained kinetic data is fed into two models, PSO and PFO, and the parameters of the kinetic model are calculated together with the correlation coefficient R^2 ; the data are summarized in Table 2 and Figure 7.

Table 2. Kinetics parameters of dyes adsorption onto 0.3 CoFe-MOF.

| Model | Parameter | Unit | MB | RhB | MO | CR |
|---------------------|-----------|---|----------|---------|----------|----------|
| Pseudo first-order | k_1 | $\text{min}^{-1}/(\text{mg/L})^{1/n}$ | 0.1766 | 0.0204 | 0.2636 | 0.28402 |
| | Q_1 | mg/g | 295.5441 | 49.7644 | 105.8228 | 164.6799 |
| | R^2 | – | 0.9732 | 0.8699 | 0.9073 | 0.9954 |
| Pseudo second-order | k_2 | $\text{g}/(\text{mg}\cdot\text{min})\cdot 10^4$ | 0.0014 | 5.5680 | 0.0050 | 0.0072 |
| | Q_2 | mg/g | 303.6247 | 55.7506 | 107.9445 | 166.5055 |
| | R^2 | – | 0.9797 | 0.9199 | 0.9967 | 0.9974 |

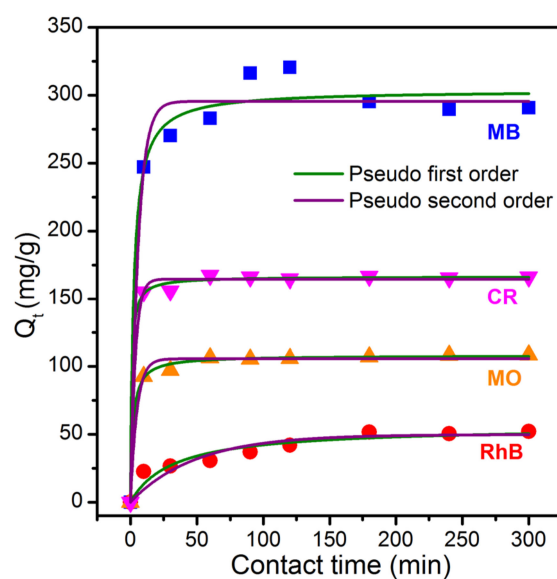


Figure 7. Adsorption kinetics for dyes onto 0.3 CoFe-MOF.

The first-order pseudo model proposes an assumption about the adsorption rate in relation to the number of unadsorbed centroids:

$$\ln(q_e - q_t) = \ln q_e - k_1 t \quad (1)$$

where k_1 is the first-order pseudo ratio (1/min), the adsorption capacity q_t at time t (min) and the equilibrium adsorption capacity q_e (mg/g) at the equilibrium time (min).

The second-order pseudo equation is used to describe the adsorption via chemisorption with the rate constant k_2 (g/mgmin). The equation is calculated as follows:

$$\frac{t}{q_t} = \frac{1}{k_2 q_e^2} + \frac{t}{q_e} \quad (2)$$

Based on the calculated data in Table 2, the correlation coefficient (R^2) for all adsorption kinetic models is very high ($R^2_{MB} = 0.9732$ and 0.9797), ($R^2_{MO} = 0.9073$ and 0.9967), ($R^2_{CR} = 0.9954$ and 0.9974), and ($R^2_{RhB} = 0.8699$ and 0.9199), respectively, showing good statistical compatibility between the surveyed data. The data results show that the dye adsorption is consistent with the pseudo second order (PSO) versus pseudo first order (PFO) model based on the correlation coefficient R^2 of PSO > PFO.

3.6. Adsorption Isotherm

To describe the monolayer adsorption behavior of materials, the Langmuir model assumes the adsorption mechanism occurs on a homogeneous surface with an infinitely large number of adsorption centers.

The following formula characterizes the Langmuir equation:

$$\frac{1}{q_e} = \frac{1}{q_m k_L} \cdot \frac{1}{C_e} + \frac{1}{q_m} \quad (3)$$

where C_e (mg/L) and q_e (mg/g) is the equilibrium concentrations and adsorption capacity, and q_m (mg/g) and K_L (L/mg) are the maximum adsorption capacity and Langmuir's constant.

The multilayer adsorption process on the heterogeneous surface is described by the Freundlich model. Accordingly, the Freundlich equation assumes the relationship between reversible adsorption and ideal adsorption occurring at different energy levels according to the following equation:

$$\ln q_e = \ln k_F + \frac{1}{n} \ln C_e \quad (4)$$

where $1/n$ and K_F [(mg/g)(L/mg) $^{1/n}$] are Freundlich coefficients related to the compatibility of the adsorption process and adsorption capacity, respectively.

The parameters of the isotherm model calculated using the nonlinear regression are listed in Table 3 and Figure 8. However, based on the R^2 value, it is clear that the experimental data are in good agreement with the Langmuir model ($R^2 = 0.99$) rather than the Freundlich model ($R^2 = 0.91$) for MB. Besides, MO with a correlation coefficient of $R^2 > 0.98$ complies with both isothermal models. For 0.3 CoFe-MOF, according to this experimental data, the CR adsorption process ($R^2 = 0.89$) follows the Langmuir model and does not fit the Freundlich model. The R^2 correlation coefficients of RhB are 0.79128 and 0.7772, showing that the experimental data do not fit both Langmuir and Freundlich models.

Table 3. Isotherm parameters of dyes adsorption onto 0.3 CoFe-MOF.

| Model | Parameter | Unit | MB | RhB | MO | CR |
|------------|-----------|------------------------|----------|---------|----------|----------|
| Langmuir | k_L | L/mg | 0.0420 | 0.1464 | 0.7009 | 1.5313 |
| | Q_m | mg/g | 600.9305 | 61.5874 | 131.9806 | 168.9234 |
| | R^2 | – | 0.99 | 0.79128 | 0.9837 | 0.89 |
| Freundlich | k_F | (mg/g)/(mg/g) $^{1/n}$ | 148.59 | 44.3143 | 124.5085 | – |
| | $1/n$ | – | 0.2428 | 0.0533 | 0.0088 | – |
| | R^2 | – | 0.91 | 0.7772 | 0.98226 | – |

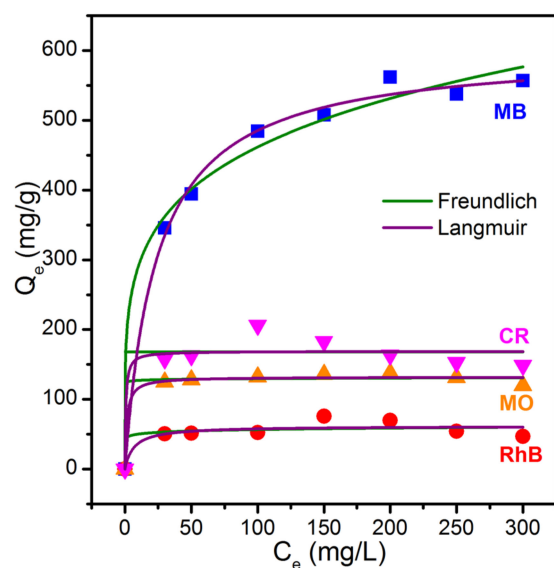


Figure 8. Adsorption isotherms for dyes onto 0.3 CoFe-MOF.

3.7. Adsorption Mechanism

Based on the factors affecting dye adsorption capacity from Fe-MOF doped Co materials, an adsorption mechanism has been proposed to better understand the mechanism of cationic and anionic dyes. The MB and RhB or MO and CR dyes usually exist as cations and anions. Therefore, the electrostatic interaction between 0.3 CoFe-MOF and the dye was used to account for the adsorption. Based on the point charge of the 0.3 CoFe-MOF material surface when the pH values are greater than pH_{Hpzc}, the 0.3 CoFe-MOF surface is negatively charged, so electrostatic repulsions will appear with the dye molecules. Cations increase the adsorption capacity [31]. In addition, the specific structure of the dye molecules is a factor affecting the adsorption process by the π - π interaction between the benzene rings in the dye molecule with 0.3 CoFe-MOF [32]. One of the factors that directly affects the ability to remove dyes is the molecular size and charge of dyes. Specifically, MO contains fewer aromatic rings than CR, and the MO anion has a smaller negative charge than CR or the linearity in the molecular formula of the MB cation in order to enhance the adsorption ability to reach the available sites on the MOF easy way [14]. Besides, the porosity of the material facilitated dye adsorption in the liquid phase due to the pore-filling interaction [33].

3.8. Adsorption of Mixed Organic Dyes

As previous studies have reported that effective dye adsorption from contaminated water depends on the charge of the MOF organic framework and the charge of the selected dyes and the cationic framework often exhibited better adsorption of anionic dyes and vice versa [14], the present study has employed 0.3 CoFe-MOF material as the adsorbent to remove the mixtures of cationic and anionic dyes in wastewater. The dye mixture is assumed experimentally as cationic and anionic dye systems (MB + MO), anionic dyes (MO + CR), and cationic dyes (MB + RhB) (Figure 9).

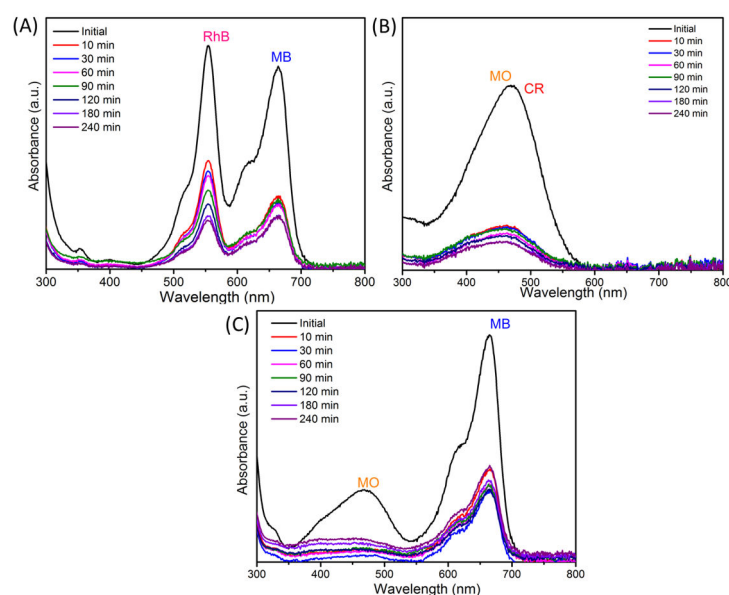


Figure 9. Dye-mixed adsorption spectra over time of 0.3 CoFe-MOF (A) RhB and MB, (B) MO and CR, and (C) MO and MB.

The adsorption process was performed following similar procedure, in which 0.01 g/L of 0.3 CoFe-MOF sample was added to an Erlenmeyer flask containing 50 mL of dye solution at a initial concentration of 30 mg/L and concentrated on a Jeiotech thermostatic shaker. After fixed periods of time, the color change of the dye was evaluated using the UV-Vis spectrum at various wavelength. Results have shown that the dye was adsorbed on the Co-doped Fe-MOF efficiently. Based on Figure 9, the dye adsorption spectra were rapidly removed after 10 min for all three mixed systems and the dye concentration continued to decline with increasing adsorption time. At 664 nm (MB) and 465 nm (MO), the maximum adsorption of both MB and MO was recorded as 70% and 81% at 30 min, respectively. On the other hand, in the mixed system of cationic dyes with a maximum adsorption at 554 nm (RhB) and 664 (MB), the removal efficiency was 56% for RhB and 67% for MB. During the 30-min reaction time of the mixed anionic dye system, the MO and CR adsorption peaks also occurred, with dye removal efficiencies of 77% (MO) and 80% (CR). When further extending the time to 240 min, the adsorption efficiency of the MB and MO mixture tended to reduce by 58% and 69%, respectively.

Similarly, the adsorption efficiency continued to increase in the mixed system of cations (74% MB and 80% RhB) and anions (85% MO and 89% CR). The spectral scanning data demonstrated that the use of 0.3 CoFe-MOF as an adsorbent in the dye mixture had effective removal on both cationic and anionic dyes. From the analysis results, it can be seen that the adsorption is affected by the charge, structure, and size of the dye [34]. For example, the CR anionic dye solution is separated from the CR and MB, CR and MO, CR and RB solution systems after two minutes in the dark by Mn(II)-MOF. High CR removal efficiency is superior to specific residual dye RB (10%) < MO (11%) < MB (18%) < CR (98%) [35]. Liu Yang et al. (2019) successfully separated a mixture of cationic (Rho 6G and MB) and anionic (AF and MO) dyes using Cd-MOF materials. The MO anionic dye was efficiently adsorbed by 100 mg of Cd-MOF from an aqueous solution containing MO and Rho 6G. Similarly, in the MB and AF dye systems, the MB cationic dye is hardly adsorbed and leaves the column [36].

4. Conclusions

An organic-inorganic hybrid of metal salts and terephthalate acid has been successfully synthesized by reacting iron (III) chloride with terephthalic acid in N,N-dimethylformamide solvent by solvothermal method. Based on the synthesis conditions on the bimetallic organic framework, CoFe-MOF was successfully synthesized at different ratios with high

order and crystallinity. The synthesized CoFe-MOF has a structural morphology, including polyhedral bars with a relatively uniform surface and contains small capillaries inside with a pore-like structure of about 2.2 nm in diameter and an area of about 2.2 nm. The specific surface area of the composite sample was 280.9 m²/g. Among four tested dyes (i.e., MB, RhB, MO, and CR), the best adsorption capacity of 0.3 CoFe-MOF was obtained upon removing MB dye (562.1 mg/g) and remained stable after 4 re-uses. Besides, 0.3 CoFe-MOF rapidly showed the highest removal efficiency towards the mixture of MO and MB within 30 min. These findings can be considered an essential platform for improving the efficiency of pigment adsorption to combat water pollution issues.

Author Contributions: Writing—original draft preparation, T.K.N.T. and T.K.O.N.; data curation, N.B.H. and T.C.Q.N.; conceptualization, N.B.H. and C.P.K.P.; methodology, L.D.T. and T.K.N.T.; formal analysis, T.C.Q.N., L.D.T. and C.P.K.P.; writing—review and editing T.K.O.N. and T.K.N.T. All authors have read and agreed to the published version of the manuscript.

Funding: The study was supported by The Youth Incubator for Science and Technology Programme, managed by Youth Development Science and Technology Center—Ho Chi Minh Communist Youth Union and Department of Science and Technology of Ho Chi Minh City, the contract number is No. 10/2021/HĐ-KHCNT-VU.

Institutional Review Board Statement: Not applicable.

Informed Consent Statement: Not applicable.

Data Availability Statement: All the data is available within the manuscript.

Conflicts of Interest: The authors declare no conflict of interest.

References

1. Furukawa, H.; Ko, N.; Go, Y.B.; Aratani, N.; Choi, S.B.; Choi, E.; Yazaydin, A.Ö.; Snurr, R.Q.; O’Keeffe, M.; Kim, J. Ultrahigh Porosity in Metal-Organic Frameworks. *Science* **2010**, *329*, 424–428. [\[CrossRef\]](#) [\[PubMed\]](#)
2. Choi, S.; Cha, W.; Ji, H.; Kim, D.; Lee, H.J.; Oh, M. Synthesis of Hybrid Metal-Organic Frameworks of {Fe_xM_yM’_{1-x-y}}-Y-MIL-88B and the Use of Anions to Control Their Structural Features. *Nanoscale* **2016**, *8*, 16743–16751. [\[CrossRef\]](#) [\[PubMed\]](#)
3. Chen, L.; Wang, H.F.; Li, C.; Xu, Q. Bimetallic Metal-Organic Frameworks and Their Derivatives. *Chem. Sci.* **2020**, *11*, 5369–5403. [\[CrossRef\]](#) [\[PubMed\]](#)
4. Li, X.; Guo, W.; Liu, Z.; Wang, R.; Liu, H. Fe-Based MOFs for Efficient Adsorption and Degradation of Acid Orange 7 in Aqueous Solution via Persulfate Activation. *Appl. Surf. Sci.* **2016**, *369*, 130–136. [\[CrossRef\]](#)
5. Shen, L.; Song, H.; Wang, C. Metal-Organic Frameworks Triggered High-Efficiency Li Storage in Fe-Based Polyhedral Nanorods for Lithium-Ion Batteries. *Electrochim. Acta* **2017**, *235*, 595–603. [\[CrossRef\]](#)
6. Van Tran, T.; Nguyen, D.T.C.; Le, H.T.N.; Vo, D.V.N.; Doan, V.D.; Dinh, V.P.; Nguyen, H.T.T.; Nguyen, T.D.; Bach, L.G. Amino-Functionalized MIL-88B(Fe)-Based Porous Carbon for Enhanced Adsorption toward Ciprofloxacin Pharmaceutical from Aquatic Solutions. *Comptes Rendus Chim.* **2019**, *22*, 804–812. [\[CrossRef\]](#)
7. Nguyen, V.; Nguyen, T.; Bach, L.; Hoang, T.; Bui, Q.; Tran, L.; Nguyen, C.; Vo, D.-V.; Do, S. Effective Photocatalytic Activity of Mixed Ni/Fe-Base Metal-Organic Framework under a Compact Fluorescent Daylight Lamp. *Catalysts* **2018**, *8*, 487. [\[CrossRef\]](#)
8. Ngan, T.T.K.; Thuy, T.B.; van Tan, L.; Nguyen, T.T. Iron-Manganese Bimetallic-Organic Framework as a Photocatalyst for Degradation of Rhodamine B Organic Dye under Visible Light. *Bull. Chem. React. Eng. Catal.* **2021**, *16*, 916–924. [\[CrossRef\]](#)
9. Ngan Tran, T.K.; Ho, H.L.; Nguyen, H.V.; Tran, B.T.; Nguyen, T.T.; Thi Bui, P.Q.; Bach, L.G. Photocatalytic Degradation of Rhodamine B in Aqueous Phase by Bimetallic Metal-Organic Framework M/Fe-MOF (M = Co, Cu, and Mg). *Open Chem.* **2022**, *20*, 52–60. [\[CrossRef\]](#)
10. Burrows, A.D. Mixed-Component Metal-Organic Frameworks (MC-MOFs): Enhancing Functionality through Solid Solution Formation and Surface Modifications. *CrystEngComm* **2011**, *13*, 3623–3642. [\[CrossRef\]](#)
11. Abednatanzi, S.; Gohari Derakhshandeh, P.; Depauw, H.; Coudert, F.X.; Vrielinck, H.; Van Der Voort, P.; Leus, K. Mixed-Metal Metal-Organic Frameworks. *Chem. Soc. Rev.* **2019**, *48*, 2535–2565. [\[CrossRef\]](#)
12. Masoomi, M.Y.; Morsali, A.; Dhakshinamoorthy, A.; Garcia, H. Mixed-Metal MOFs: Unique Opportunities in Metal-Organic Framework (MOF) Functionality and Design. *Angew. Chem. Int. Ed.* **2019**, *58*, 15188–15205. [\[CrossRef\]](#)
13. Molavi, H.; Hakimian, A.; Shojaei, A.; Raeiszadeh, M. Selective Dye Adsorption by Highly Water Stable Metal-Organic Framework: Long Term Stability Analysis in Aqueous Media. *Appl. Surf. Sci.* **2018**, *445*, 424–436. [\[CrossRef\]](#)
14. Mantasha, I.; Saleh, H.A.M.; Qasem, K.M.A.; Shahid, M.; Mehtab, M.; Ahmad, M. Efficient and Selective Adsorption and Separation of Methylene Blue (MB) from Mixture of Dyes in Aqueous Environment Employing a Cu(II) Based Metal Organic Framework. *Inorganica Chim. Acta* **2020**, *511*, 119787. [\[CrossRef\]](#)

15. Deng, S.Q.; Mo, X.J.; Zheng, S.R.; Jin, X.; Gao, Y.; Cai, S.L.; Fan, J.; Zhang, W.G. Hydrolytically Stable Nanotubular Cationic Metal-Organic Framework for Rapid and Efficient Removal of Toxic Oxo-Anions and Dyes from Water. *Inorg. Chem.* **2019**, *58*, 2899–2909. [\[CrossRef\]](#)
16. Akansha, K.; Chakraborty, D.; Sachan, S.G. Decolorization and Degradation of Methyl Orange by *Bacillus Stratosphericus* SCA1007. *Biocatal. Agric. Biotechnol.* **2019**, *18*, 101044. [\[CrossRef\]](#)
17. Naseem, K.; Farooqi, Z.H.; Begum, R.; Irfan, A. Removal of Congo Red Dye from Aqueous Medium by Its Catalytic Reduction Using Sodium Borohydride in the Presence of Various Inorganic Nano-Catalysts: A Review. *J. Clean. Prod.* **2018**, *187*, 296–307. [\[CrossRef\]](#)
18. Khan, I.; Saeed, K.; Zekker, I.; Zhang, B.; Hendi, A.H.; Ahmad, A.; Ahmad, S.; Zada, N.; Ahmad, H.; Shah, L.A.; et al. Review on Methylene Blue: Its Properties, Uses, Toxicity and Photodegradation. *Water* **2022**, *14*, 242. [\[CrossRef\]](#)
19. Laramie, M.D.; Smith, M.K.; Marmarchi, F.; McNally, L.R.; Henary, M. Small Molecule Optoacoustic Contrast Agents: An Unexplored Avenue for Enhancing in Vivo Imaging. *Molecules* **2018**, *23*, 2766. [\[CrossRef\]](#)
20. Saig, Z.M. Various Adsorbents for Removal of Rhodamine B Dye: A Review. *Indones. J. Chem.* **2021**, *21*, 1039. [\[CrossRef\]](#)
21. Ding, L.; Zeng, M.; Wang, H.; Jiang, X.B. Synthesis of MIL-101-Derived Bimetal-Organic Framework and Applications for Lithium-Ion Batteries. *J. Mater. Sci. Mater. Electron.* **2021**, *32*, 1778–1786. [\[CrossRef\]](#)
22. Xie, Q.; Li, Y.; Lv, Z.; Zhou, H.; Yang, X.; Chen, J.; Guo, H. Effective Adsorption and Removal of Phosphate from Aqueous Solutions and Eutrophic Water by Fe-Based MOFs of MIL-101. *Sci. Rep.* **2017**, *7*, 3316. [\[CrossRef\]](#)
23. Guan, H.; Wang, N.; Feng, X.; Bian, S.; Li, W.; Chen, Y. FeMn Bimetallic MOF Directly Applicable as an Efficient Electrocatalyst for Overall Water Splitting. *Colloids Surf. Physicochem. Eng. Asp.* **2021**, *624*, 126596. [\[CrossRef\]](#)
24. Chen, L.; Zuo, X.; Zhou, L.; Huang, Y.; Yang, S.; Cai, T.; Ding, D. Efficient Heterogeneous Activation of Peroxymonosulfate by Facilely Prepared Co/Fe Bimetallic Oxides: Kinetics and Mechanism. *Chem. Eng. J.* **2018**, *345*, 364–374. [\[CrossRef\]](#)
25. Wu, Y.; Liu, Z.; Bakhtari, M.F.; Luo, J. Preparation of GO/MIL-101(Fe,Cu) Composite and Its Adsorption Mechanisms for Phosphate in Aqueous Solution. *Environ. Sci. Pollut. Res.* **2021**, *28*, 51391–51403. [\[CrossRef\]](#)
26. Yang, L.X.; Yang, J.C.E.; Fu, M.L. Magnetic CoFe₂O₄ Nanocrystals Derived from MIL-101 (Fe/Co) for Peroxymonosulfate Activation toward Degradation of Chloramphenicol. *Chemosphere* **2021**, *272*, 129567. [\[CrossRef\]](#)
27. Wang, Z.; Wu, C.; Zhang, Z.; Chen, Y.; Deng, W.; Chen, W. Bimetallic Fe/Co-MOFs for Tetracycline Elimination. *J. Mater. Sci.* **2021**, *56*, 15684–15697. [\[CrossRef\]](#)
28. Shakly, M.; Saad, L.; Seliem, M.K.; Bonilla-Petriciolet, A.; Shehata, N. New Insights into the Selective Adsorption Mechanism of Cationic and Anionic Dyes Using MIL-101(Fe) Metal-Organic Framework: Modeling and Interpretation of Physicochemical Parameters. *J. Contam. Hydrol.* **2022**, *247*, 103977. [\[CrossRef\]](#)
29. Van Tran, T.; Nguyen, D.T.C.; Le, H.T.N.; Bach, L.G.; Vo, D.V.N.; Dao, T.U.T.; Lim, K.T.; Nguyen, T.D. Effect of Thermolysis Condition on Characteristics and Nonsteroidal Anti-Inflammatory Drugs (NSAIDs) Absorbability of Fe-MIL-88B-Derived Mesoporous Carbons. *J. Environ. Chem. Eng.* **2019**, *7*, 103356. [\[CrossRef\]](#)
30. Hejazi, R.; Mahjoub, A.R.; Khavar, A.H.C.; Khazaei, Z. Fabrication of Novel Type Visible-Light-Driven TiO₂@ MIL-100 (Fe) Microspheres with High Photocatalytic Performance for Removal of Organic Pollutants. *J. Photochem. Photobiol. Chem.* **2020**, *400*, 112644. [\[CrossRef\]](#)
31. Lin, S.; Song, Z.; Che, G.; Ren, A.; Li, P.; Liu, C.; Zhang, J. Adsorption Behavior of Metal-Organic Frameworks for Methylene Blue from Aqueous Solution. *Microporous Mesoporous Mater.* **2014**, *193*, 27–34. [\[CrossRef\]](#)
32. Paiman, S.H.; Rahman, M.A.; Uchikoshi, T.; Abdullah, N.; Othman, M.H.D.; Jaafar, J.; Abas, K.H.; Ismail, A.F. Functionalization Effect of Fe-Type MOF for Methylene Blue Adsorption. *J. Saudi Chem. Soc.* **2020**, *24*, 896–905. [\[CrossRef\]](#)
33. Haque, E.; Jun, J.W.; Jhung, S.H. Adsorptive Removal of Methyl Orange and Methylene Blue from Aqueous Solution with a Metal-Organic Framework Material, Iron Terephthalate (MOF-235). *J. Hazard. Mater.* **2011**, *185*, 507–511. [\[CrossRef\]](#) [\[PubMed\]](#)
34. Kaur, H.; Kumar, R.; Kumar, A.; Krishnan, V.; Koner, R.R. Trifunctional Metal-Organic Platform for Environmental Remediation: Structural Features with Peripheral Hydroxyl Groups Facilitate Adsorption, Degradation and Reduction Processes. *Dalton Trans.* **2019**, *48*, 915–927. [\[CrossRef\]](#)
35. Liu, J.; Zhang, X.-Y.; Hou, J.-X.; Liu, J.-M.; Jing, X.; Li, L.-J.; Du, J.-L. Functionalized Mn(II)-MOF Based on Host-Guest Interaction for Selective and Rapid Capture of Congo Red from Water. *J. Solid State Chem.* **2019**, *270*, 697–704. [\[CrossRef\]](#)
36. Yang, L.; Liu, Y.-L.; Liu, C.-G.; Fu, Y.; Ye, F. A Cationic Metal-Organic Framework for Dye Adsorption and Separation Based on Column-Chromatography. *J. Mol. Liq.* **2020**, *300*, 112311. [\[CrossRef\]](#)